Published in final edited form as:
Dev Cell. 2010 July 20; 19(1): 138–147. doi:10.1016/j.devcel.2010.06.008.

Epidermal wound repair is regulated by the planar cell polarity signaling pathway

Jacinta Caddy[1], **Tomasz Wilanowski**[1], **Charbel Darido**[1], **Sebastian Dworkin**[1], **Stephen B. Ting**[2], **Quan Zhao**[1], **Gerhard Rank**[1], **Alana Auden**[1], **Seema Srivastava**[1], **Tony A. Papenfuss**[3], **Jennifer N. Murdoch**[4], **Patrick O. Humbert**[2], **Nidal Boulos**[5], **Thomas Weber**[6], **Jian Zuo**[6], **John M. Cunningham**[5], and **Stephen M. Jane**[1,7,*]

[1] Rotary Bone Marrow Research Laboratories, c/o Royal Melbourne Hospital Post Office, Grattan Street, Parkville, VIC 3050, Australia

[2] Cell Cycle and Cancer Genetics Laboratory, Peter MacCallum Cancer Centre, Melbourne, VIC 3002, Australia

[3] Division of Bioinformatics, The Walter and Eliza Hall Institute, Parkville, VIC 3050, Australia

[4] MRC Mammalian Genetics Unit, Harwell, Oxfordshire, OX11 UK

[5] Department of Pediatrics, University of Chicago, Chicago IL, 60637 USA

[6] Department of Developmental Neurobiology, St. Jude Children's Research Hospital, Memphis TN, 38105 USA

[7] Department of Medicine, University of Melbourne, Parkville, Victoria 3050, Australia

SUMMARY

The mammalian PCP pathway regulates diverse developmental processes requiring coordinated cellular movement, including neural tube closure and cochlear stereociliary orientation. Here, we show that epidermal wound repair is regulated by PCP signaling. Mice carrying mutant alleles of PCP genes *Vangl2*, *Celsr1*, *PTK7*, and *Scrb1*, and the transcription factor *Grhl3*, interact genetically, exhibiting failed wound healing, neural tube defects and disordered cochlear polarity. Using phylogenetic analysis, ChIP, and gene expression in *Grhl3*$^{-/-}$ mice, we identified *RhoGEF19*, a homologue of a RhoA activator involved in PCP signaling in *Xenopus*, as a direct target of GRHL3. Knockdown of *Grhl3* or *RhoGEF19* in keratinocytes induced defects in actin polymerisation, cellular polarity and wound healing, and re-expression of *RhoGEF19* rescued these defects in *Grhl3*-kd cells. These results define a role for *Grhl3* in PCP signaling, and broadly implicate this pathway in epidermal repair.

Highlights

- *Grhl3* is a component of the PCP signaling pathway
- *Grhl3* acts in this pathway through the RhoA activator, *RhoGEF19*
- PCP signalling regulates mammalian embryonic epidermal wound repair

*Correspondence: jane@wehi.edu.au; phone 61-3-93428641; Fax 61-3-93428634.

INTRODUCTION

The PCP pathway governs a diverse range of cellular and developmental events that require coordinated orientation and movement of cells within a plane of epithelium (Axelrod and McNeill, 2002; Seifert and Mlodzik, 2007; Wu and Mlodzik, 2009; Zallen, 2007). In *Drosophila*, PCP is evident in the organization of cuticular structures, such as wing hairs and body bristles, and in the ommatidial clusters of the eye (Adler, 2002; Klein and Mlodzik, 2005). PCP signaling occurs through the serpentine receptor *frizzled* (*fz*), and requires the cytoplasmic factors *dishevelled* (*dsh*), and *prickle* (*pk*), the transmembrane protein *Van Gogh/Strabismus* (*Vang/Stbm*), the cadherin *starry night/flamingo* (*stan/fmi*), and the Ankyrin repeat protein *Diego* (*Dgo*), known collectively as the core PCP proteins (Adler, 2002; Seifert and Mlodzik, 2007). Downstream of these core factors are effector molecules that act in many distinct contexts. These include the small GTPases of the Rho subfamily (*RhoA* and *Rac1*), and the *Rho-associated kinase* (*rok*) that provide essential links to the actin cytoskeleton (Fanto et al., 2000; Strutt et al., 1997; Winter et al., 2001).

In vertebrates, the epidermis provides a conspicuous example of PCP, as evidenced by the pattern of scales, feathers and hairs in different organisms. The organization of internal tissues is also dependent on this pathway, as demonstrated by the regimented orientation of stereocilia of the sensory hair cells of the cochlea (Curtin et al., 2003; Dabdoub et al., 2003; Montcouquiol et al., 2003). The process of narrowing and lengthening the embryonic axis in gastrulation and neurulation by convergent extension (CE) has also been linked to the PCP pathway, with all of the vertebrate homologs of *Drosophila* core PCP genes, and many of the downstream effectors implicated in this process (Keller, 2002; Wallingford et al., 2000). In addition, vertebrate genes that lack *Drosophila* homologs involved in PCP, such as *PTK7* (Lu et al., 2004), have been shown to exhibit defects in CE. In mice, perturbed CE may result in a shortened longitudinal embryonic axis, craniorachischisis, in which the neural tube fails to close from the hindbrain to the most caudal extremity of the embryo (Curtin et al., 2003; Hamblet et al., 2002; Kibar et al., 2001), and diminished elongation of the cochlea, resulting in misorientation of stereocilia (Wang et al., 2005).

Mammalian wound healing is another process requiring coordinated cell movement in the plane of epithelia (Martin and Parkhurst, 2004). Integral to this process is regulation of the actin cytoskeleton mediated through the small Rho GTPases (Brock et al., 1996; Fukata et al., 2003; Van Aelst and Symons, 2002). The small GTPases also play a critical role in PCP signaling in both *Drosophila* and vertebrates (Habas et al., 2001; Strutt et al., 1997; Yan et al., 2009), leading to the hypothesis that the PCP pathway could be important for epidermal repair. This hypothesis was strengthened with the analysis of mice lacking the *Grainy head-like 3* (*Grhl3*) gene. *Grhl3* is a member of a family of developmental transcription factors that includes the *Drosophila* gene *grainy head* (*grh*), which is essential for the *fz* pathway, and has also been implicated wound healing in the fly (Lee and Adler, 2004; Mace et al., 2005; Wilanowski et al., 2002; Ting et al., 2003a). Mice lacking *Grhl3* exhibit severe NTD (Ting et al., 2003b), and a marked disturbance in formation, maintenance and repair of the epidermal barrier (Ting et al., 2005). Based on these findings, we postulated that *Grhl3* was a component of the mammalian PCP pathway, and that this pathway may regulate epidermal wound healing in mammals.

RESULTS

Grhl3 and *Vangl2* interact genetically in neural tube closure and cochlear hair cell orientation

The NTD in mice lacking *Grhl3* is accompanied by marked shortening of their longitudinal axis, and a widened midline (see Figures S1A, S1B available online) (Ting et al., 2003b).

Similar, but more severe morphological appearances are observed in many of the mouse mutants of PCP genes including, *Vangl2* (mutated in the *loop-tail* (*Lp*) mouse (Kibar et al., 2001)); *Scrb1*, (mutated in the *circletail* (*Crc*) mouse (Murdoch et al., 2003)); *Celsr1*, (mutated in the *spin cycle* (*Scy*) and *crash* (*Crsh*) mice (Curtin et al., 2003)); double null mutants of two of the *Dishevelled* (*Dvl*) genes ($Dvl1^{-/-}/Dvl2^{-/-}$) (Hamblet et al., 2002); and *PTK7* (Lu et al., 2004). In view of these phenotypic similarities, and the known role of *grh* in PCP (Lee and Adler, 2004), we interbred $Grhl3^{+/-}$ mice, which display no neural tube, skin barrier or wound healing defects, with $Vangl2^{+/-}$ mice, which exhibit a loop of the tail and rarely, low sacral spina bifida (Murdoch et al., 2001). We observed that 67% of the $Vangl2^{+/-}/Grhl3^{+/-}$compound heterozygotes harvested between embryonic day (E) 15.5 and E18.5 exhibited NTD that were lumbo-sacral or high sacral spina bifida (Figure 1A, left embryo). This effect was specific, as no $Vangl2^{+/+}/Grhl3^{+/-}$embryos exhibited NTD (Figure 1A, right embryo). In 87% of the $Vangl2^{+/-}/Grhl3^{+/+}$ embryos, we observed a loop tail alone phenotype (Figure 1A, middle embryo), with the remaining 13% exhibiting very low sacral spina bifida (data not shown). The cumulative results of these intercrosses are shown in Figure 1B. This trans-heterozygous interaction suggests that *Grhl3* and *Vangl2* may function in a common genetic pathway to regulate PCP. This interaction appears less strong than that reported between $Vangl2^{+/-}$ and $Scrb1^{+/-}$ embryos, where a subset of mice display craniorachischisis (Montcouquiol et al., 2003), but is similar to the interaction between *Vangl2* and *PTK7*, which also manifests as incompletely penetrant spina bifida (Lu et al., 2004).

Another key function of the mammalian PCP genes is to co-ordinate the orientation of the actin-based stereociliary bundles of the sensory hair cells in the organ of Corti (Dabdoub et al., 2003). Analysis of *LacZ* staining in the cochleae of $Grhl3^{+/-}$ mice, which carry a β-galactosidase gene fused in frame to the twelfth codon of exon 2 of the *Grhl3* gene as part of the gene targeting strategy (Ting et al., 2003b), revealed expression in the inner and outer hair cell layers (Figure 1C). We therefore tested whether mice deficient for *Grhl3* or $Vangl2^{+/-}/Grhl3^{+/-}$ compound heterozygotes exhibited abnormal stereociliary bundle orientation. In wild type mice, every stereociliary bundle is oriented towards the abneural side of the sensory epithelium. Examination of the cochleae from *Grhl3*-null mice revealed that the regular organization of one row of inner hair cells (IHC) and three rows of outer hair cells (OHCs) separated by pillar cells was preserved (data not shown). Similarly, cochleae from $Vangl2^{+/-}/Grhl3^{+/+}$ (Figure 1D) and $Vangl2^{+/+}/Grhl3^{+/-}$ (Figure 1E) animals displayed normal orientation of all hair cell layers. In contrast, cochleae from $Vangl2^{+/-}/Grhl3^{+/-}$ animals displayed abnormal bundle orientation throughout the basal, middle and apical turns (Figure 1F). Although the defects were most pronounced in the third row of the OHCs (OHC3), with some bundles rotated 180^0 from the wild type position (Figure 1G), the IHC, OHC1 and OHC2 rows also exhibited abnormal orientation (Figure 1H). Overall, the hair bundle phenotype of the $Vangl2^{+/-}/Grhl3^{+/-}$ cochleae was less severe than observed with $Vangl2^{-/-}$ mutants, particularly in the IHC row (Montcouquiol et al., 2003), but more pronounced than either the *Scrb1* (Montcouquiol et al., 2003) or *PTK7* (Lu et al., 2004) mutants.

Defective wound healing in PCP mutants

In view of the wound healing defects observed in the *Grhl3*-deficient mice, and the parallels in coordinated cellular movement in PCP and wound repair, we postulated that mice mutant for other PCP genes may also exhibit defective wound healing *in vivo*. *In situ* hybridisation studies have previously demonstrated expression of *Vangl2* in the embryonic epidermis (Devenport and Fuchs, 2008; Murdoch et al., 2003), and multiple partial *Vangl2* cDNA clones have been isolated from adult epidermis. To examine wound healing in $Vangl2^{-/-}$ mutant mice, and *Vangl2/Grhl3* compound heterozygotes, we harvested mutant embryos of

both genotypes and their littermates with their yolk sac intact at E12.5 (to assess early embryonic wound healing, which involves contraction of a cable of filamentous actin at the wound edge, and is scarless), and E16.5 (to assess late embryonic wound healing, in which keratinocytes crawl inwards to close the wound, as also occurs in adults (Martin, 1997; Redd et al., 2004). After wounding, the embryos were cultured for up to 24 hours in roller bottles and then analysed by scanning electron microscopy (SEM). Under these *ex vivo* conditions the embryos are viable and continue to develop (McCluskey and Martin, 1995), and time course experiments showed progressive closure occurred across the 24 hour period (Figure S2A). As shown in Figure 2A, at E12.5 wild type, *Vangl2*$^{+/-}$, *Vangl2*$^{-/-}$, *Vangl2*$^{+/-}$/*Grhl3*$^{+/+}$, and *Vangl2*$^{+/+}$/*Grhl3*$^{+/-}$ embryos exhibited complete wound closure after 24 hours. In contrast, the *Vangl2*$^{+/-}$/*Grhl3*$^{+/-}$ mutant embryos displayed defective wound repair at 24 hours. The results obtained with all litters examined are presented in Table 1, and the differences between the *Vangl2*$^{+/-}$/*Grhl3*$^{+/-}$ embryos and all other genotypes were statistically significant. In the wound repair assays at E16.5, *Vangl2*$^{+/-}$/*Grhl3*$^{+/-}$ embryos also displayed defective healing (Figure 2B) that was not observed with the other genotypes.

To determine whether defective wound healing was observed in other PCP mutant strains, we initially assessed the *Crc* (*Scrb1*) mutant line. Expression of the defective gene in this line, *Scrb1* has been demonstrated in embryonic skin (Murdoch et al., 2003), and multiple partial *Scrb1* cDNA clones have been isolated from adult epidermis. We examined wound healing in E12.5 *Scrb1*$^{-/-}$embryos, *Scrb1/Grhl3* compound heterozygote embryos, and their littermate controls (Figure 2C). In most *Scrb1*$^{+/-}$, *Scrb1*$^{+/+}$/*Grhl3*$^{+/-}$, *Scrb1*$^{+/-}$/*Grhl3*$^{+/+}$, and wild type embryos complete wound closure was observed after 24 hours. In contrast, the *Scrb1*$^{-/-}$and *Scrb1*$^{+/-}$/*Grhl3*$^{+/-}$ embryos displayed a failure of wound closure at 24 hours. Failed wound healing has also been observed in another *Scrb1* mutant line, the *rumpelstiltzchen* (*rumz*/Line90) mice (Zarbalis et al., 2004). The results obtained with all litters examined are presented in Table 1, and the differences between the *Scrb1*$^{+/-}$/*Grhl3*$^{+/-}$ and *Scrb1*$^{-/-}$embryos and all other genotypes were statistically significant. In addition to the wound healing defects, all *Scrb1*$^{-/-}$embryos displayed craniorachischisis, as reported previously (Murdoch et al., 2001). Interestingly, the *Scrb1*$^{+/-}$/*Grhl3*$^{+/-}$embryos did not exhibit any NTD (data not shown). To determine whether genetic interactions between PCP genes other than *Grhl3* manifested with impaired wound healing, we intercrossed *Vangl2*$^{+/-}$ and *Scrb1*$^{+/-}$ mice (Figure S2B). Healing proceeded normally in wild type, *Vangl2*$^{+/-}$/*Scrb1*$^{+/+}$, and *Vangl2*$^{+/+}$/*Scrb1*$^{+/-}$ embryos. In contrast, the *Vangl2*$^{+/-}$/*Scrb1*$^{+/-}$ embryos failed to heal. The results obtained with all litters examined are presented in Table S1, and the differences between the *Vangl2*$^{+/-}$/*Scrb1*$^{+/-}$ embryos and all other genotypes were statistically significant. We extended these studies by examining wound healing at E12.5 in *PTK7*-mutant mice and the *Crash* (*Celsr1* mutant) line (Figure S2C). In both, wild type and heterozygous embryos healed normally, but null embryos exhibited defective wound repair (Table S1). The defect in the *Celsr1*$^{-/-}$mice was less penetrant, with 54% of the embryos exhibiting open wounds after 24 hours, and the remaining 46% demonstrating partial or complete closure. These findings confirm that the integrity of the PCP signaling pathway is essential for early and late embryonic wound repair.

In addition to its role in epidermal repair, we have previously demonstrated that *Grhl3* is pivotal for the formation of the epidermal barrier in mammals through the regulation of the enzyme involved in cross linking structural proteins and lipids, transglutaminase 1 (Ting et al., 2005). This function appears to be independent of its role in the PCP pathway, as both the *Vangl2*$^{+/-}$/*Grhl3*$^{+/-}$ and *Scrb1*$^{+/-}$/*Grhl3*$^{+/-}$ compound heterozygous mice exhibited normal barrier function (data not shown).

Grhl3 acts through the Rho guanine nucleotide exchange factor, *RhoGEF19*

To explore the role of *Grhl3* in PCP signaling and wound repair, we initially examined the expression of known PCP genes in our *Grhl3*-null mice, and the levels of *Grhl3* in the PCP mutants (Figure S3). No changes were observed in either setting. To identify potential target genes, we utilised the previously defined GRHL3 DNA consensus binding site (5'-AA**C**CG**G**TT-3') (Ting et al., 2005) to interrogate a customised dataset of genomic regions located within 10kb of gene transcriptional start sites that are highly conserved in placental mammals (see Experimental procedures). Consistent with our expression data, no sites were identified in the regulatory regions of *Vangl2*, *Scrb1*, *PTK7*, and *Celsr1*. However, we did identify a site that was absolutely conserved in all species in the proximal promoter region of the *RhoGEF19* gene, situated 109 base pairs (bp) upstream of the murine, and 137 bp upstream of the human transcription start sites (Figure S4A). Mouse *RhoGEF19* is a homolog of the *Xenopus* and human *WGEF* genes that have been shown to preferentially activate RhoA (Tanegashima et al., 2008; Wang et al., 2004). In addition, *XWGEF* has recently been shown to be a component of the PCP pathway, and involved in the regulation of CE (Tanegashima et al., 2008). We confirmed specific binding of GRHL3 to the *RhoGEF19* site *in vitro* in electrophoretic mobility shift assays (EMSA) (Figure 3A), and *in vivo* by chromatin immunoprecipitation (ChIP) (Figure 3B). Consistent with *RhoGEF19* being a direct target of GRHL3, expression of the gene was markedly reduced in the epidermis of *Grhl3*-null mice. *RhoGEF19* expression in the dermis, (where *Grhl3* is not expressed) was not altered (Figure 3C), and nor was it altered in the other PCP mutant strains (Figure S4B). Q-PCR with epidermal and dermal-specific genes confirmed the integrity of the samples (data not shown). We therefore examined the effects of GRHL3 expression on RhoA activation in the presence, and absence of *RhoGEF19* using pull down assays with glutathione-S-transferase (GST) fusion of the Rhotekin Rho-binding domain (RBD) to detect RhoA-GTP. HEK293T cells were co-transfected with a lentivirus carrying an short hairpin RNA (shRNA) targeting *RhoGEF19* (*RhoGEF19-kd*), or a scrambled control shRNA (Scr) and an mammalian expression vector carrying HA-tagged GRHL3, or the control empty vector. Expression of HA-GRHL3 was confirmed by Western blot (Figure 3D, IB:α-HA). A marked increase in active RhoA was detected in the Scr cells expressing GRHL3 compared to Scr cells transfected with vector alone. This increase was completely abrogated in the *RhoGEF19-kd* cells despite robust expression of HA-GRHL3 in these cells. Consistent with these findings, we showed that expression of *RhoGEF19* was increased in the GRHL3-transfected Scr cells by Q-PCR (as no antibody is available for RhoGEF19), but remained low in the *RhoGEF19-kd* cells transfected with HA-GRHL3 (Figure 3E, graph).

To directly examine the importance of *RhoGEF19* in wound repair, we utilized the shRNA lentivirus to target the *RhoGEF19* transcript in the human keratinocyte cell line, HaCAT. We confirmed a knockdown of approximately 80% by Q-RT-PCR (Figure 4A) compared to cells transduced with a scrambled control shRNA (Scr). The *RhoGEF19*-kd HaCAT cells failed to "heal" in scratch assays (20% closure), unlike the Scr cells, which migrated to completely close the scratch within 24 hours (Figure 4B). Activated RhoA was also reduced in these cells (Figure 4C). To confirm that *RhoGEF19* was a critical GRHL3 target gene in wound repair, we generated HaCAT cells expressing an shRNA targeting *Grhl3* (*Grhl3*-kd), and a scrambled control line (Scr). Expression of *Grhl3* in the *Grhl3*-kd cells was reduced to less than 20% of the Scr control at both RNA (Figure 4D), and protein level (Figure 4D, inset). *RhoGEF19* expression was also reduced to less than 25% in these cells compared to Scr control (Figure 4G). Scratch assays with these cell lines displayed almost complete healing with the Scr control cells (94%), but persistence of the "wound" in the *Grhl3*-kd cells (17% closure) (Figure 4E). This was not attributable to reduced cell growth, as these cells, and *Grhl3*$^{-/-}$keratinocytes, exhibit enhanced proliferation compared to their wild type counterparts (Ting et al., 2005, and not shown). Consistent with our previous data, activated

RhoA was reduced in the *Grhl3*-kd cells (Figure 4F). To determine if re-expression of *RhoGEF19* could rescue the wound defect in *Grhl3*-kd cells, we transfected these cells with a mammalian expression vector containing the *RhoGEF19* cDNA (*Grhl3*-kd + *RhoGEF19*), or the empty vector as a control (*Grhl3*-kd + Vector). *RhoGEF19* expression levels were restored to near wild type in the *Grhl3*-kd + *RhoGEF19* cells (Figure 4G). Scratch assays with these cells demonstrated that re-expression of *RhoGEF19* substantially rescued the wound healing phenotype observed with the *Grhl3*-kd cells (10% closure versus 73%) (Figure 4H). Taken together, this data identifies *RhoGEF19* as a critical direct target of *Grhl3* in the context of epidermal migration in wound repair.

Grhl3 and *RhoGEF19* regulate actin polymerisation and cellular polarity during wound repair

To further explore the mechanism underpinning defective epidermal migration in the absence of *Grhl3* or *RhoGEF19*, we initially examined wound repair in cultured *Grhl3*-null embryos. A hallmark of wound closure at E12.5 is the formation of a “purse-string” actin cable around the wound margin. Examination of *LacZ* staining in wounded $Grhl3^{+/-}$ and $Grhl3^{-/-}$embryos demonstrated a marked induction of circumferential expression between 0 and 18 hours (Figure 5A), suggesting that increased *Grhl3* expression in response to wounding would result in enhanced *RhoGEF19* expression at the wound margins. Whole mount rhodamine-phalloidin staining of F-actin fibers in wild type and $Grhl3^{-/-}$embryos revealed marked differences, with clear actin polymerisation and purse string formation in controls, compared with disorganized structure at the wound margins in the mutants (Figure 5B). To examine this further, we compared the effects of loss of *Grhl3* and *Rho GEF 19* expression on actin polymerisation in human *Grhl3*-kd, *RhoGEF19*-kd and Scr control keratinocytes in scratch assays after 18 hours (Figure 5C). The Scr cells, which migrate to completely heal the scratch after 24 hours, displayed extensive actin stress fibers associated with cellular projections aligned in the direction of the migrating cells. In contrast, both the *Grhl3*-kd, and to an even greater extent, *RhoGEF19*-kd cells formed only rudimentary stress fibers that showed irregular organization and were not directed towards the scratched area.

Cells at the leading edge of a wound polarize the nucleus, actin cytoskeleton, and microtubule organizing centre (MTOC)/Golgi network in the axis of migration (Hall, 2005). We analyzed the polarity of leading edge cells 6 hours following scratch wounding of human *Grhl3*-kd, *RhoGEF19*-kd, and Scr control keratinocytes (Figure 5D). In 90% of Scr cells at the wound edge, the Golgi was polarized within a 120^0 arc in front of the nucleus. In contrast, both *Grhl3*-kd, and *RhoGEF19*-kd cells showed no polarization, and the Golgi remained essentially randomly distributed around the nucleus. This finding is similar to the cellular polarity defects we have previously observed with shRNA-mediated knockdown of *Scribble* in the context of wounding in MCF10A cells (Dow et al., 2007). To determine the importance of loss of *Grhl3* and *RhoGEF19* expression on cell polarity at the wound margin, we transfected the human *Grhl3*-kd, and *RhoGEF19*-kd keratinocytes with a mammalian expression vector containing a constitutively active form of RhoA, (G14V RhoA) (Ren et al., 1999), tagged with the *myc* epitope, or the empty vector control, and performed scratch assays (Figure 5E). Both knockdown cell lines transfected with the empty vector failed to heal over 24 hours (17% and 30% closure), and this was not altered with the expression of G14V RhoA, indicating that non-polarized activation of RhoA is insufficient to rescue the wound closure defects observed with loss of *Grhl3* or *RhoGEF19*. Scr control cells transfected with G14V RhoA healed less completely than cells transfected with vector alone (100% versus 75%), and *myc* expression was equivalent across transfections (Figure S5).

In summary, our data defines *RhoGEF19* as a direct *Grhl3* target gene that is essential for polarized RhoA activation, epidermal migration and wound repair, in the context of the PCP signalling pathway (Figure 5F).

DISCUSSION

Three important findings have emerged from our studies: 1) early and late embryonic epidermal wound healing in mammals is regulated by the PCP signaling pathway; 2) *Grhl3* is a component of this pathway, acting through the RhoA activator, *RhoGEF19*; 3) regulation of expression of *RhoGEFs* by tissue-restricted transcription factors provides a mechanism for spatio-temporal-specific remodelling of the actin cytoskeleton, and selective cell migration.

Integral to both PCP and wound repair is the need for cells to adopt an axis of polarity, followed by reorganisation of their cytoskeleton leading to directional migration. Consistent with this, regulators of the actin cytoskeleton including RhoA, Rho-associated kinase, and Rac1 have been implicated in both processes (Kodama et al., 2004; Strutt et al., 1997; Tscharntke et al., 2007; Vaezi et al., 2002; Winter et al., 2001). Our data identifies epidermal wound repair defects with five PCP mutant alleles, either in the homozygous state (*PTK7*, *Celsr1*, *Scrb1*, *Grhl3*), or as compound heterozygotes (*Vangl2/Scrb1*, *Vangl2/Grhl3*). The variation in wound healing observed with different mutant alleles is similar to the phenotypic heterogeneity seen with other PCP-regulated processes in various mutant strains, and suggests that the obligate genes required for the diverse processes governed by PCP signaling are context-specific. For wound repair, *PTK7*, *Scrb1* and *Grhl3* are all essential, whereas *Vangl2* is redundant, and loss of *Celsr1* appears to be partially compensated. In cochlear stereociliary organization, *Vangl2*/*Scrb1* compound heterozygotes exhibit marked polarity defects, whereas *PTK7/Vangl2* compound heterozygotes have normal cochleas, despite abnormalities in both *Vangl2*$^{-/-}$and *PTK7*-null embryos (Lu et al., 2004; Montcouquiol et al., 2003). In neural tube closure, almost all *PTK7/Vangl2* compound heterozygotes display spina bifida (similar to the *Grhl3/Vangl2* mice), but only 50% of *Vangl2*/*Scrb1* mutants exhibit craniorachischisis (Murdoch et al., 2001). These findings may be attributable to subtle differences in the PCP pathways regulating the individual processes, or alternatively, variations in the protein complexes involved in wound repair, stereociliary polarity and neurulation.

Several genes implicated in cell motility in response to wounding have also been linked to the PCP pathway. In *Drosophila*, mutants of *Twinstar* the homolog of cofilin/ADF (actin depolymerization factor), a key regulator of actin dynamics at the leading edge of motile cells (DesMarais et al., 2005), display polarity defects in the wing, eye and other epithelia (Blair et al., 2006). Although cofilin/ADF has not yet been implicated in mammalian PCP, it is noteworthy that mice lacking cofilin-1, the predominant protein isoform expressed in the embryo, exhibit craniorachischisis, a hallmark of many PCP mutants (Gurniak et al., 2005). In mice, the secreted glycoprotein, Cthrc1 promotes cell migration at wound margins by reducing the deposition of the collagen matrix (Durmus et al., 2006; Pyagay et al., 2005). This factor also functions as a *Wnt* cofactor, selectively activating the PCP pathway in the context of neural tube closure and cochlear stereociliary organization (Yamamoto et al., 2008). Vangl1 has been linked to epithelial repair in the intestine (Kalabis et al., 2006), and Rho-associated kinase 1 (ROCK-1) is essential for accumulation of filamentous actin in closure of the eyelids and ventral body wall (Shimizu et al., 2005), and has also been implicated in assembly of the stratified epidermis, which may be important for wound repair (Vaezi et al., 2002). Interestingly, several PCP mutants, and the *Grhl3*-null mice also exhibit defects in eyelid closure at birth (Curtin et al., 2003; Hislop et al., 2008; Lu et al., 2004; Montcouquiol et al., 2003; Yu et al., 2008).

Grhl3 functions as a key transcriptional regulator in the mammalian PCP signaling pathway. It interacts genetically with the core PCP gene *Vangl2*, in regulating closure of the neural tube, and orientation of the stereociliary bundles of the cochlea, typical features of other

recently described PCP genes (Lu et al., 2004; Yamamoto et al., 2008). Unlike many of the other homozygous mutant PCP strains, which exhibit craniorachischisis, and cochlea polarity defects, *Grhl3*-null animals display thoraco-lumbo-sacral spina bifida (Ting et al., 2003b), and have normal stereociliary bundles. These findings are reminiscent of the phenotypes observed with another PCP gene, *Dvl2*, one of the three mammalian homologs of the *Drosophila dsh* gene. In isolation, loss of *Dvl2* expression results in thoracic spina bifida (Hamblet et al., 2002), but stereociliary bundle polarity is unaffected (Wang et al., 2005). Only in the context of *Dvl1/2* double mutant embryos, or $Dvl2^{-/-}$/Lp/+ embryos was complete failure of neural tube closure (Hamblet et al., 2002), and stereociliary polarity defects (Wang et al., 2005) observed. The presence of two highly related mammalian homologs of *Grhl3* suggests that some functional redundancy also exists in this gene family (Wilanowski et al., 2002).

The identification of *Grhl3* as a PCP gene, analogous to its *Drosophila* homologue *grh*, further extends the parallels between fly and mammalian PCP signaling. Homologues of all the *Drosophila* core PCP genes have been identified in vertebrates, and implicated in PCP regulated developmental events (Seifert and Mlodzik, 2007). Mutants of *grh* display polarity defects of wing hairs and ommatidia, and abnormal localisation of planar polarity proteins in the wing cells. In addition, *grh* interacts genetically with several of the *fz* pathway genes, including *Vang/Stbm* (Lee and Adler, 2004). Reduced levels of Stan protein in both larval wing discs and pupal wings in *grh* mutants suggests that this factor may also transcriptionally regulate *stan/fmi*, although putative binding sites for Grh were not evident in the *stan/fmi* regulatory regions (Lee and Adler, 2004). In mice, *Grhl3* interacts genetically with *Vangl2*, a homologue of *Vang/Stbm*, but we found no evidence that homologues of *stan/fmi* (*Celsr1-3*) were direct target genes of GRHL3. No predicted binding sites for GRHL3 were identified in the *Celsr* promoters (or any of the other PCP genes examined), and expression of all these genes was not altered in the *Grhl3*-null mice.

The key GRHL3 target gene that we did identify was the RhoA activator, *RhoGEF19*. The *Xenopus* homologue of this gene, *WGEF* specifically activates RhoA, and co-localizes with *Dvl* at the plasma membrane in a *fz*-dependent manner. Upon *Wnt* signaling and *fz* activation, *Dvl*, *Daam-1* and *Rho* are recruited to the cell membrane (Kim and Han, 2007; Park et al., 2006), where they are co-localized and complexed with *XWGEF*, leading to Rho activation (Tanegashima et al., 2008). Morpholino-induced loss of *WGEF* expression results in defective CE, with embryos displaying shortened axes, and in severe cases, neural tube defects (Tanegashima et al., 2008). In mouse epidermis, loss of *Grhl3* led to a marked reduction in *RhoGEF19* expression, with loss of actin polymerisation and defective cellular polarisation and migration at the wound margins. Re-expression of *RhoGEF19* in *Grhl3*-kd cells rescues wound healing indicating that *RhoGEF19* is an essential *Grhl3* target gene in this process. It is likely that transcriptional regulation of *RhoGEF19* will also be important for other *Grhl3*-dependent morphogenetic events, such as neural tube and eyelid closure.

EXPERIMENTAL PROCEDURES

Experimental Animals

The generation and genotyping of *Grhl3* mice has been described previously (Ting et al., 2003b). *Lp/+* mice of the LPT/LeJ stock were obtained from the Jackson Laboratory. *Crc*, *Crash and PTK7* mutant mice were obtained from Dr Jennifer Murdoch. Mouse genotyping is detailed in the Supplemental data. All experiments were pre-approved by The University of Melbourne Animal Ethics Committee.

Stereociliary Analysis

Cochleae from E18.5 embryos were dissected and whole mounts from the organ of Corti were prepared. PCP was analyzed by staining for the kinocilium using an anti-acetylated tubulin antibody (Sigma-Aldrich, St.Louis, MO, USA) and filamentous actin was labeled with rhodamine-conjugated phalloidin (Molecular Probes, Eugene, OR, USA). The orientation of individual stereociliary bundles was determined as described previously (Montcouquiol et al., 2003). Data was collected from a minimum of three samples for each genotype.

Embryonic wound healing assays

Analysis of wound repair was performed on embryonic day 12.5 and 16.5 embryos as described previously (McCluskey and Martin, 1995). At least 6 embryos of each genotype were analysed for wound closure. Failed wound repair was defined as a residual defect >80% of the original wound diameter. A Fischer's Exact Test was used to determine statistical difference between wound healing for the different genotypes. P values ≤ 0.05 were considered significant, and results were analysed using the computer software program Prism (GraphPad). The skin permeability assays and histological analysis were performed as described previously (Ting et al., 2005).

Identification of conserved elements in promoter regions

Conserved elements upstream of human genes were identified using annotation data from the UCSC genome browser (http://genome.ucsc.edu/; NCBI Build 36.1). From this, we constructed a new dataset consisting of 10kb regions upstream of the transcription start sites of human RefSeq genes. We then took the intersection of these regions with predicted conserved elements that were identified using a phylo-hidden Markov model, PhastCons (Siepel et al., 2005), on the placental mammal-subset of the 28-way multiple alignment of vertebrate genomes. The resulting 178,611 predicted conserved elements located in upstream regions had a median length of 28nt. The sequence data contained in these elements was then extracted to a fasta file and searched using the GRHL3 DNA binding consensus sequence.

ChIP and EMSA

ChIP was performed as described previously (Wilanowski et al., 2008). EMSAs were performed using recombinant mouse GRHL3 protein, and the *Grhl3* DNA consensus binding sequence, as defined previously (Ting et al., 2005). Primer and oligonucleotide sequences for each assay are detailed in the Supplemental data.

RNA preparation and Q-PCR

For expression analysis from skin, the epidermis was separated from dermis using 2 mg/ml Dispase II (Invitrogen, Carlsbad, CA, USA) at 4°C overnight. Both tissues were homogenised in TRIzol (Invitrogen) and RNA extracted according to the manufacturer's instructions. For expression analysis in the human embryonic kidney cell line (HEK) 293T, cells were co-transfected with the pcDNA3.1 expression vector (Invitrogen) containing hemagglutinin (HA) epitope-tagged murine *Grhl3*, and an MSCV-based GFP expressing vector using Fugene (Roche, Basel, Switzerland). After 48 hours, GFP+ cells were sorted by FACS and total RNA was extracted using TriZol. Q-PCR carried out as described previously (Ting et al., 2003b) and primer sequences are detailed in the Supplemental data. A student's t-test was used to determine statistical difference in expression levels. P values ≤ 0.05 were considered significant, and results were analysed using the computer software program Prism (GraphPad). The error bars in all expression analyses represent the standard error of the mean.

Activation Assay

Activation assays were performed using Cytoskeleton kits (Cytoskeleton Inc., Denver, CO, USA) in accordance to the manufacturers specifications, as detailed in the Supplemental data. Each experiment in this study was performed in triplicate on at least three separate occasions (n≥9), with parallel control and experimental treatments.

Scratch Assays and Actin Analysis

Scratch assays and phalloidin staining of cultured keratinocyte lines were performed as described previously (Hislop et al., 2008), as detailed in the Supplemental data. Each experiment was performed in triplicate on at least three separate occasions with parallel controls.

RNA interference, lentiviral infection and transduction

The shRNA target oligonucleotides for *RhoGEF19* and the scrambled (Scr) control were cloned into the LentiLox3.7 (pLL3.7) lentiviral vector (ATCC, Manassas, VA, USA) using the *Hpa*I and *Xho*I sites. The shRNA target oligonucleotides for *Grhl3* were cloned into the pSUPER.retro.neo+GFP vector using the *Bgl*II and *Hind*III sites. The target sequences and generation of viruses are detailed in the Supplemental data.

Supplementary Material

Refer to Web version on PubMed Central for supplementary material.

Acknowledgments

We thank Andrew Copp for *Crc* mice, Gordon Smyth for statistical analyses, Mary Corbett, Sumitha Vasudevan, Sarah King, and James Pickles for technical assistance. Animal support was provided by staff from the Bio21 and Walter & Eliza Hall Institutes. SMJ is a Principal Research Fellow of the Australian National Health and Medical Research Council (NHMRC). POH is supported by a career development award from the NHMRC. The work was supported by Project Grants from the NHMRC, and The March of Dimes Foundation (SMJ); the Deafness Research Foundation, and the National Institutes of Health (USA) (JZ).

References

Adler PN. Planar signaling and morphogenesis in Drosophila. Dev Cell. 2002; 2:525–535. [PubMed: 12015961]

Axelrod JD, McNeill H. Coupling planar cell polarity signaling to morphogenesis. Scientific World Journal. 2002; 2:434–454. [PubMed: 12806028]

Blair A, Tomlinson A, Pham H, Gunsalus KC, Goldberg ML, Laski FA. Twinstar, the Drosophila homolog of cofilin/ADF, is required for planar cell polarity patterning. Development. 2006; 133:1789–1797. [PubMed: 16571634]

Brock J, Midwinter K, Lewis J, Martin P. Healing of incisional wounds in the embryonic chick wing bud: characterization of the actin purse-string and demonstration of a requirement for Rho activation. J Cell Biol. 1996; 135:1097–1107. [PubMed: 8922389]

Curtin JA, Quint E, Tsipouri V, Arkell RM, Cattanach B, Copp AJ, Henderson DJ, Spurr N, Stanier P, Fisher EM, et al. Mutation of Celsr1 disrupts planar polarity of inner ear hair cells and causes severe neural tube defects in the mouse. Curr Biol. 2003; 13:1129–1133. [PubMed: 12842012]

Dabdoub A, Donohue MJ, Brennan A, Wolf V, Montcouquiol M, Sassoon DA, Hseih JC, Rubin JS, Salinas PC, Kelley MW. Wnt signaling mediates reorientation of outer hair cell stereociliary bundles in the mammalian cochlea. Development. 2003; 130:2375–2384. [PubMed: 12702652]

DesMarais V, Ghosh M, Eddy R, Condeelis J. Cofilin takes the lead. J Cell Sci. 2005; 118:19–26. [PubMed: 15615780]

Devenport D, Fuchs E. Planar polarization in embryonic epidermis orchestrates global asymmetric morphogenesis of hair follicles. Nat Cell Biol. 2008; 10:1257–1268. [PubMed: 18849982]

Dow LE, Kauffman JS, Caddy J, Peterson AS, Jane SM, Russell SM, Humbert PO. The tumour-suppressor Scribble dictates cell polarity during directed epithelial migration: regulation of Rho GTPase recruitment to the leading edge. Oncogene. 2007; 26:2272–2282. [PubMed: 17043654]

Durmus T, LeClair RJ, Park KS, Terzic A, Yoon JK, Lindner V. Expression analysis of the novel gene collagen triple helix repeat containing-1 (Cthrc1). Gene Expr Patterns. 2006; 6:935–940. [PubMed: 16678498]

Fanto M, Weber U, Strutt DI, Mlodzik M. Nuclear signaling by Rac and Rho GTPases is required in the establishment of epithelial planar polarity in the Drosophila eye. Curr Biol. 2000; 10:979–988. [PubMed: 10985385]

Fukata M, Nakagawa M, Kaibuchi K. Roles of Rho-family GTPases in cell polarisation and directional migration. Curr Opin Cell Biol. 2003; 15:590–597. [PubMed: 14519394]

Gurniak CB, Perlas E, Witke W. The actin depolymerizing factor n-cofilin is essential for neural tube morphogenesis and neural crest cell migration. Dev Biol. 2005; 278:231–241. [PubMed: 15649475]

Habas R, Kato Y, He X. Wnt/Frizzled activation of Rho regulates vertebrate gastrulation and requires a novel Formin homology protein Daam1. Cell. 2001; 107:843–854. [PubMed: 11779461]

Hall A. Rho GTPases and the control of cell behaviour. Biochem Soc Trans. 2005; 33:891–895. [PubMed: 16246005]

Hamblet NS, Lijam N, Ruiz-Lozano P, Wang J, Yang Y, Luo Z, Mei L, Chien KR, Sussman DJ, Wynshaw-Boris A. Dishevelled 2 is essential for cardiac outflow tract development, somite segmentation and neural tube closure. Development. 2002; 129:5827–5838. [PubMed: 12421720]

Hislop NR, Caddy J, Ting SB, Auden A, Vasudevan S, King SL, Lindeman GJ, Visvader JE, Cunningham JM, Jane SM. Grhl3 and Lmo4 play coordinate roles in epidermal migration. Dev Biol. 2008; 321:263–272. [PubMed: 18619436]

Kalabis J, Rosenberg I, Podolsky DK. Vangl1 protein acts as a downstream effector of intestinal trefoil factor (ITF)/TFF3 signaling and regulates wound healing of intestinal epithelium. J Biol Chem. 2006; 281:6434–6441. [PubMed: 16410243]

Keller R. Shaping the vertebrate body plan by polarized embryonic cell movements. Science. 2002; 298:1950–1954. [PubMed: 12471247]

Kibar Z, Vogan KJ, Groulx N, Justice MJ, Underhill DA, Gros P. Ltap, a mammalian homolog of Drosophila Strabismus/Van Gogh, is altered in the mouse neural tube mutant Loop-tail. Nat Genet. 2001; 28:251–255. [PubMed: 11431695]

Kim GH, Han JK. Essential role for beta-arrestin 2 in the regulation of Xenopus convergent extension movements. EMBO J. 2007; 26:2513–2526. [PubMed: 17476309]

Klein TJ, Mlodzik M. Planar cell polarization: An emerging model points in the right direction. Annu Rev Cell Dev Biol. 2005; 21:155–176. [PubMed: 16212491]

Kodama A, Lechler T, Fuchs E. Coordinating cytoskeletal tracks to polarize cellular movements. J Cell Biol. 2004; 167:203–207. [PubMed: 15504907]

Lee H, Adler PN. The grainy head transcription factor is essential for the function of the frizzled pathway in the Drosophila wing. Mech Dev. 2004; 121:37–49. [PubMed: 14706698]

Lu X, Borchers AG, Jolicoeur C, Rayburn H, Baker JC, Tessier-Lavigne M. PTK7/CCK-4 is a novel regulator of planar cell polarity in vertebrates. Nature. 2004; 430:93–98. [PubMed: 15229603]

Mace KA, Pearson JC, McGinnis W. An epidermal barrier wound repair pathway in Drosophila is mediated by grainy head. Science. 2005; 308:381–385. [PubMed: 15831751]

Martin P. Wound healing--aiming for perfect skin regeneration. Science. 1997; 276:75–81. [PubMed: 9082989]

Martin P, Parkhurst SM. Parallels between tissue repair and embryo morphogenesis. Development. 2004; 131:3021–3034. [PubMed: 15197160]

McCluskey J, Martin P. Analysis of the tissue movements of embryonic wound healing--DiI studies in the limb bud stage mouse embryo. Dev Biol. 1995; 170:102–114. [PubMed: 7601301]

Montcouquiol M, Rachel RA, Lanford PJ, Copeland NG, Jenkins NA, Kelley MW. Identification of Vangl2 and Scrb1 as planar polarity genes in mammals. Nature. 2003; 423:173–177. [PubMed: 12724779]

Murdoch JN, Henderson DJ, Doudney K, Gaston-Massuet C, Phillips HM, Paternotte C, Arkell R, Stanier P, Copp AJ. Disruption of scribble (Scrb1) causes severe neural tube defects in the circletail mouse. Hum Mol Genet. 2003; 12:87–98. [PubMed: 12499390]

Murdoch JN, Rachel RA, Shah S, Beermann F, Stanier P, Mason CA, Copp AJ. Circletail, a new mouse mutant with severe neural tube defects: chromosomal localization and interaction with the loop-tail mutation. Genomics. 2001; 78:55–63. [PubMed: 11707073]

Park E, Kim GH, Choi SC, Han JK. Role of PKA as a negative regulator of PCP signaling pathway during Xenopus gastrulation movements. Dev Biol. 2006; 292:344–357. [PubMed: 16490187]

Pyagay P, Heroult M, Wang Q, Lehnert W, Belden J, Liaw L, Friesel RE, Lindner V. Collagen triple helix repeat containing 1, a novel secreted protein in injured and diseased arteries, inhibits collagen expression and promotes cell migration. Circ Res. 2005; 96:261–268. [PubMed: 15618538]

Redd MJ, Cooper L, Wood W, Stramer B, Martin P. Wound healing and inflammation: embryos reveal the way to perfect repair. Philos Trans R Soc Lond B Biol Sci. 2004; 359:777–784. [PubMed: 15293805]

Ren XD, Kiosses WB, Schwartz MA. Regulation of the small GTP-binding protein Rho by cell adhesion and the cytoskeleton. EMBO J. 1999; 18:578–585. [PubMed: 9927417]

Seifert JR, Mlodzik M. Frizzled/PCP signalling: a conserved mechanism regulating cell polarity and directed motility. Nat Rev Genet. 2007; 8:126–138. [PubMed: 17230199]

Shimizu Y, Thumkeo D, Keel J, Ishizaki T, Oshima H, Oshima M, Noda Y, Matsumura F, Taketo MM, Narumiya S. ROCK-I regulates closure of the eyelids and ventral body wall by inducing assembly of actomyosin bundles. J Cell Biol. 2005; 168:941–953. [PubMed: 15753128]

Siepel A, Bejerano G, Pedersen JS, Hinrichs AS, Hou M, Rosenbloom K, Clawson H, Spieth J, Hillier LW, Richards S, et al. Evolutionarily conserved elements in vertebrate, insect, worm, and yeast genomes. Genome Res. 2005; 15:1034–1050. [PubMed: 16024819]

Strutt DI, Weber U, Mlodzik M. The role of RhoA in tissue polarity and Frizzled signalling. Nature. 1997; 387:292–295. [PubMed: 9153394]

Tanegashima K, Zhao H, Dawid IB. WGEF activates Rho in the Wnt-PCP pathway and controls convergent extension in Xenopus gastrulation. EMBO J. 2008; 27:606–617. [PubMed: 18256687]

Ting SB, Caddy J, Hislop N, Wilanowski T, Auden A, Zhao LL, Ellis S, Kaur P, Uchida Y, Holleran WM, et al. A homolog of Drosophila grainy head is essential for epidermal integrity in mice. Science. 2005; 308:411–413. [PubMed: 15831758]

Ting SB, Wilanowski T, Cerruti L, Zhao LL, Cunningham JM, Jane SM. The identification and characterization of human Sister-of-Mammalian Grainyhead (SOM) expands the grainyhead-like family of developmental transcription factors. Biochem J. 2003a; 370:953–962. [PubMed: 12549979]

Ting SB, Wilanowski T, Auden A, Hall M, Voss AK, Thomas T, Parekh V, Cunningham JM, Jane SM. Inositol- and folate-resistant neural tube defects in mice lacking the epithelial-specific factor Grhl-3. Nat Med. 2003b; 9:1513–1519. [PubMed: 14608380]

Tscharntke M, Pofahl R, Chrostek-Grashoff A, Smyth N, Niessen C, Niemann C, Hartwig B, Herzog V, Klein HW, Krieg T, et al. Impaired epidermal wound healing in vivo upon inhibition or deletion of Rac1. J Cell Sci. 2007; 120:1480–1490. [PubMed: 17389689]

Vaezi A, Bauer C, Vasioukhin V, Fuchs E. Actin cable dynamics and Rho/Rock orchestrate a polarized cytoskeletal architecture in the early steps of assembling a stratified epithelium. Dev Cell. 2002; 3:367–381. [PubMed: 12361600]

Van Aelst L, Symons M. Role of Rho family GTPases in epithelial morphogenesis. Genes Dev. 2002; 16:1032–1054. [PubMed: 12000787]

Wallingford JB, Rowning BA, Vogeli KM, Rothbacher U, Fraser SE, Harland RM. Dishevelled controls cell polarity during Xenopus gastrulation. Nature. 2000; 405:81–85. [PubMed: 10811222]

Wang J, Mark S, Zhang X, Qian D, Yoo SJ, Radde-Gallwitz K, Zhang Y, Lin X, Collazo A, Wynshaw-Boris A, et al. Regulation of polarized extension and planar cell polarity in the cochlea by the vertebrate PCP pathway. Nat Genet. 2005; 37:980–985. [PubMed: 16116426]

Wang Y, Suzuki H, Yokoo T, Tada-Iida K, Kihara R, Miura M, Watanabe K, Sone H, Shimano H, Toyoshima H, et al. WGEF is a novel RhoGEF expressed in intestine, liver, heart, and kidney. Biochem Biophys Res Commun. 2004; 324:1053–1058. [PubMed: 15485661]

Wilanowski T, Caddy J, Ting SB, Hislop NR, Cerruti L, Auden A, Zhao LL, Asquith S, Ellis S, Sinclair R, et al. Perturbed desmosomal cadherin expression in grainy headlike 1-null mice. EMBO J. 2008; 27:886–897. [PubMed: 18288204]

Wilanowski T, Tuckfield A, Cerruti L, O'Connell S, Saint R, Parekh V, Tao J, Cunningham JM, Jane SM. A highly conserved novel family of mammalian developmental transcription factors related to Drosophila grainyhead. Mech Dev. 2002; 114:37–50. [PubMed: 12175488]

Winter CG, Wang B, Ballew A, Royou A, Karess R, Axelrod JD, Luo L. Drosophila Rho-associated kinase (Drok) links Frizzled-mediated planar cell polarity signaling to the actin cytoskeleton. Cell. 2001; 105:81–91. [PubMed: 11301004]

Wu J, Mlodzik M. A quest for the mechanism regulating global planar cell polarity of tissues. Trends Cell Biol. 2009; 19:295–305. [PubMed: 19560358]

Yamamoto S, Nishimura O, Misaki K, Nishita M, Minami Y, Yonemura S, Tarui H, Sasaki H. Cthrc1 selectively activates the planar cell polarity pathway of Wnt signaling by stabilizing the Wnt-receptor complex. Dev Cell. 2008; 15:23–36. [PubMed: 18606138]

Yan J, Lu Q, Fang X, Adler PN. Rho1 has multiple functions in Drosophila wing planar polarity. Dev Biol. 2009; 333:186–199. [PubMed: 19576201]

Yu Z, Bhandari A, Mannik J, Pham T, Xu X, Andersen B. Grainyhead-like factor Get1/Grhl3 regulates formation of the epidermal leading edge during eyelid closure. Dev Biol. 2008; 319:56–67. [PubMed: 18485343]

Zallen JA. Planar polarity and tissue morphogenesis. Cell. 2007; 129:1051–1063. [PubMed: 17574020]

Zarbalis K, May SR, Shen Y, Ekker M, Rubenstein JL, Peterson AS. A focused and efficient genetic screening strategy in the mouse: identification of mutations that disrupt cortical development. PLoS Biol. 2004; 2:E219. [PubMed: 15314648]

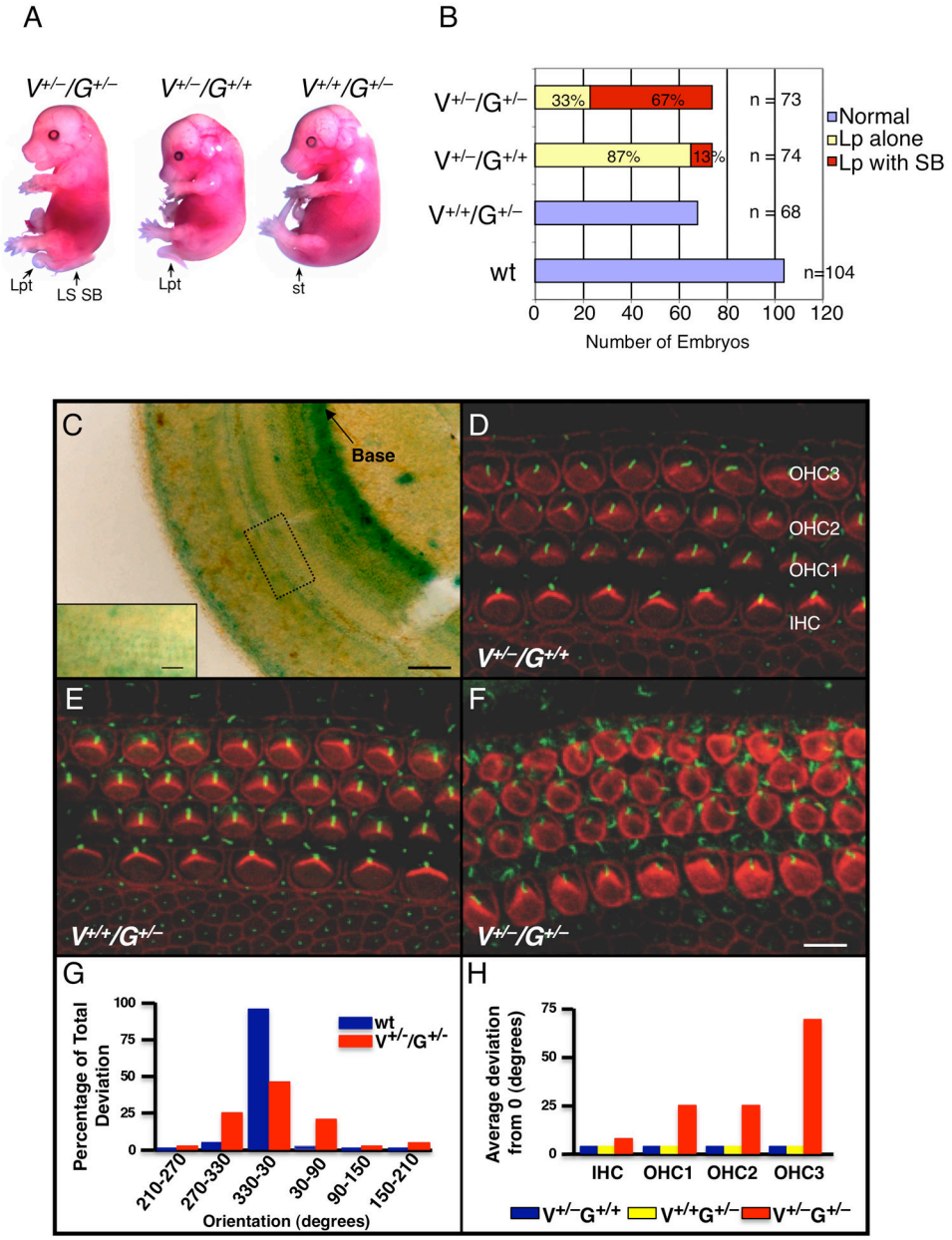

Figure 1.

Genetic interaction between *Grhl3* (G) and *Vangl2* (V) in neural tube closure and cochlear stereociliary bundle orientation. (A) E15.5 littermates from *Vangl2*$^{+/-}$/*Grhl3*$^{+/-}$matings. Lp: loop tail; LS SB: lumbo-sacral spina bifida; st: straight tail. (B) Summary of the incidence of spina bifida in the *Vangl2/Grhl3* compound heterozygotes. A total of 319 embryos from 46 separate litters of *Vangl2* and *Grhl3* heterozygote matings were analysed. (C) Section of an entire cochlear duct from a *Grhl3*$^{+/-}$ embryo at E18.5 stained with β-galactosidase. Inset is high magnification of the boxed region, illustrating the *LacZ* expressing hair cell layers. (D-F) Luminal surface of the organ of Corti in the middle turn of cochleae from E18.5 embryos with the indicated genotypes. Stereociliary bundles (red) and kinocilia (green) on IHC and OHC are uniformly orientated in (D) and (E). Bundles are non-uniform in (F) with some rotated by greater than 90^{0}. The kinocilia are also frequently mispositioned in (F). (G) Distribution histograms of OHC3 bundle orientation in wild type and *Vangl2*$^{+/-}$/*Grhl3*$^{+/-}$

cochleae. Wild type OHCs orientations are largely confined to a 60^0 segment centered on a line parallel to the neural-abneural axis. In contrast the distributions are noticeably broader in *Vangl2*$^{+/-}$*/Grhl3*$^{+/-}$ mice. (H) Average deviations from a line parallel to the neural-abneural axis for all hair cell layers in the genotypes shown in (D-F). See also Figure S1.

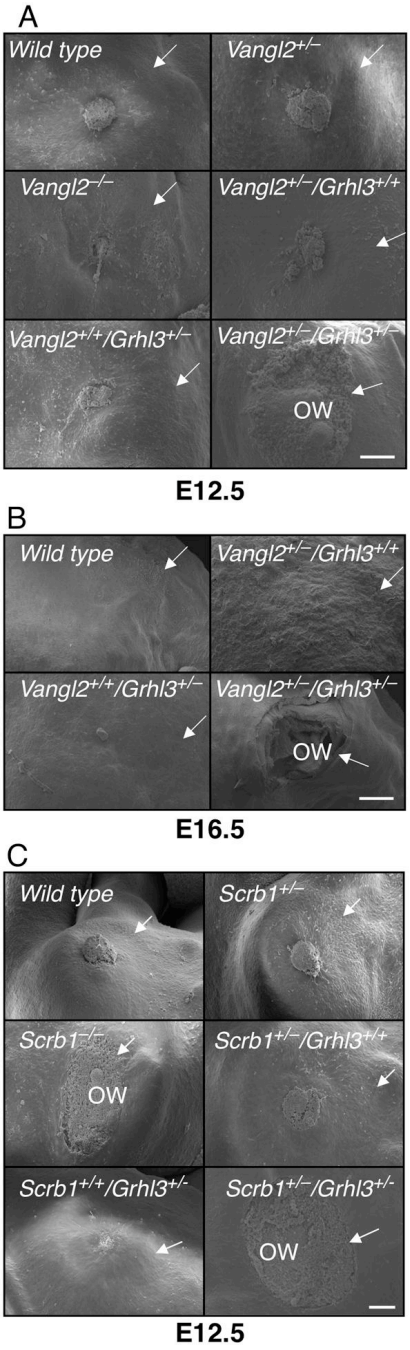

Figure 2.

Failed wound healing in PCP mutant mice. SEM of a hind limb amputation wound in embryos with the stated genotypes at (A) E12.5; (B) E16.5; and (C) E12.5. All images are representative of at least six embryos of each genotype. Wounds were classified as open if the residual defect after 24 hours culture was >80% of the original wound diameter. Arrows point to the boundary of the wound. ow - open wound. Scale = 100 μm. See also Figure S2 and Table S1.

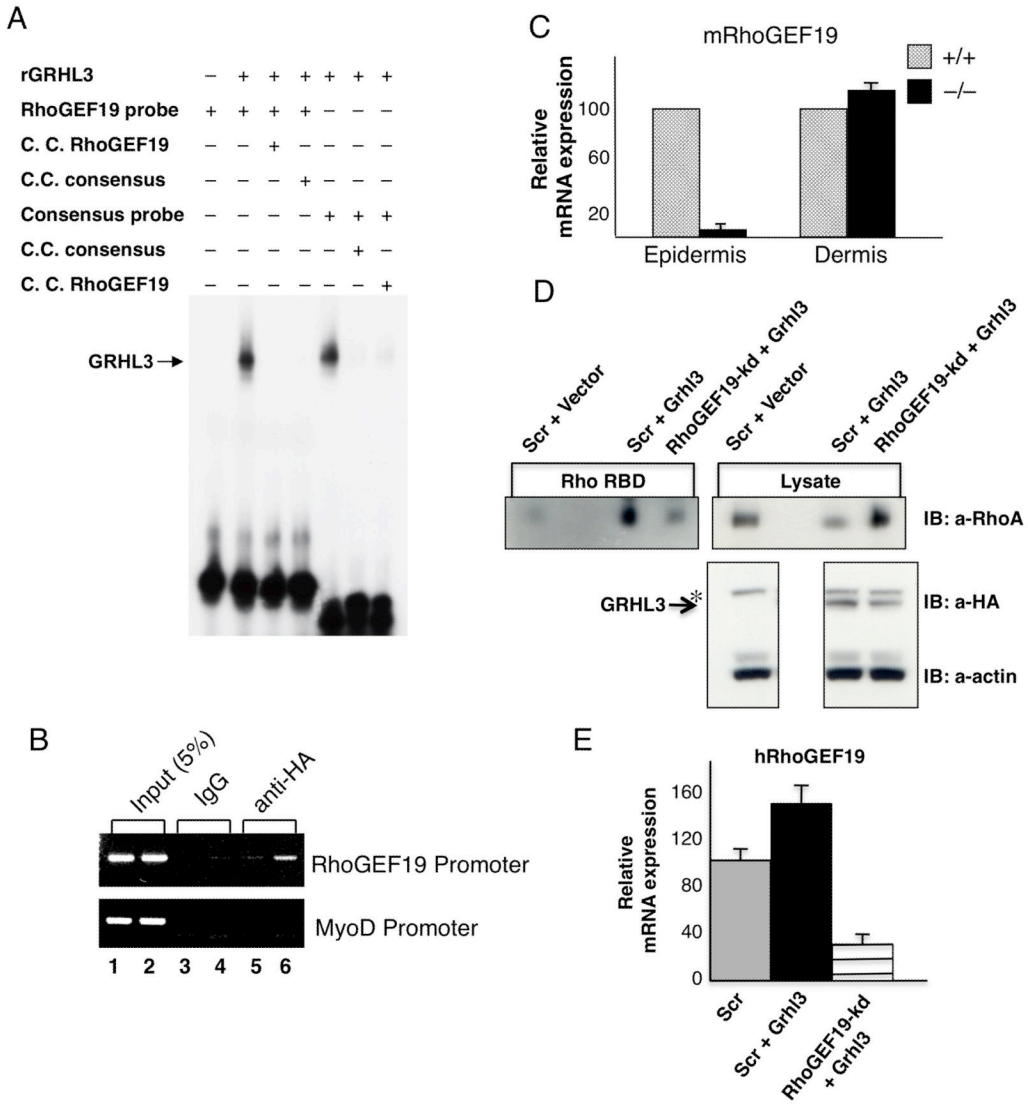

Figure 3.

RhoGEF19 is a direct target gene of GRHL3. (A) EMSA of recombinant (r) GRHL3 binding to the *RhoGEF19* promoter. A 100-fold molar excess of unlabelled cold competitor probe was added in the indicated lanes. The migration of the specific GRHL3/DNA complexes is arrowed. (B) ChIP analysis of GRHL3 on the *RhoGEF19* promoter. Chromatin from HEK 293T cells transfected with empty vector (lane 5) or HA-tagged *Grhl3* (lane 6) was immunoprecipitated using antisera to the HA-tag. As negative controls, we used pre-immune sera (lanes 3 and 4). Lane 1 and 2 shows the input chromatin. The immunoprecipitated chromatin was amplified with *RhoGEF19*, or control *MyoD* primers. (C) Q-PCR of *RhoGEF19* expression in wild type (hatched boxes) and $Grhl3^{-/-}$ (closed boxes) E18.5 epidermis and dermis. Bars represent standard errors. The *HPRT* levels served as a reference. (D, E) GRHL3 induced RhoA activation in HEK 293T cells is mediated through increased *RhoGEF19* expression. HA-tagged *Grhl3* was transfected into HEK 293T cells transduced with an shRNA to *RhoGEF19*, or a Scrambled control shRNA (Scr), and expression of HA-GRHL3 was confirmed by Western blot (IB:α-HA, α-actin loading control). GTP-Rho was precipitated using GST-RBD and detected by anti-RhoA antibody (IB:αRhoA). Total RhoA was also detected in lysates with anti-RhoA antibody. HA-GRHL3

is arrowed. *non-specific band with HA antibody. Expression of human *RhoGEF19* in Scr control cells, Scr cells expressing HA-GRHL3, and *RhoGEF19*-kd cells expressing HA-GRHL3 was determined by Q-PCR. See also Figure S3.

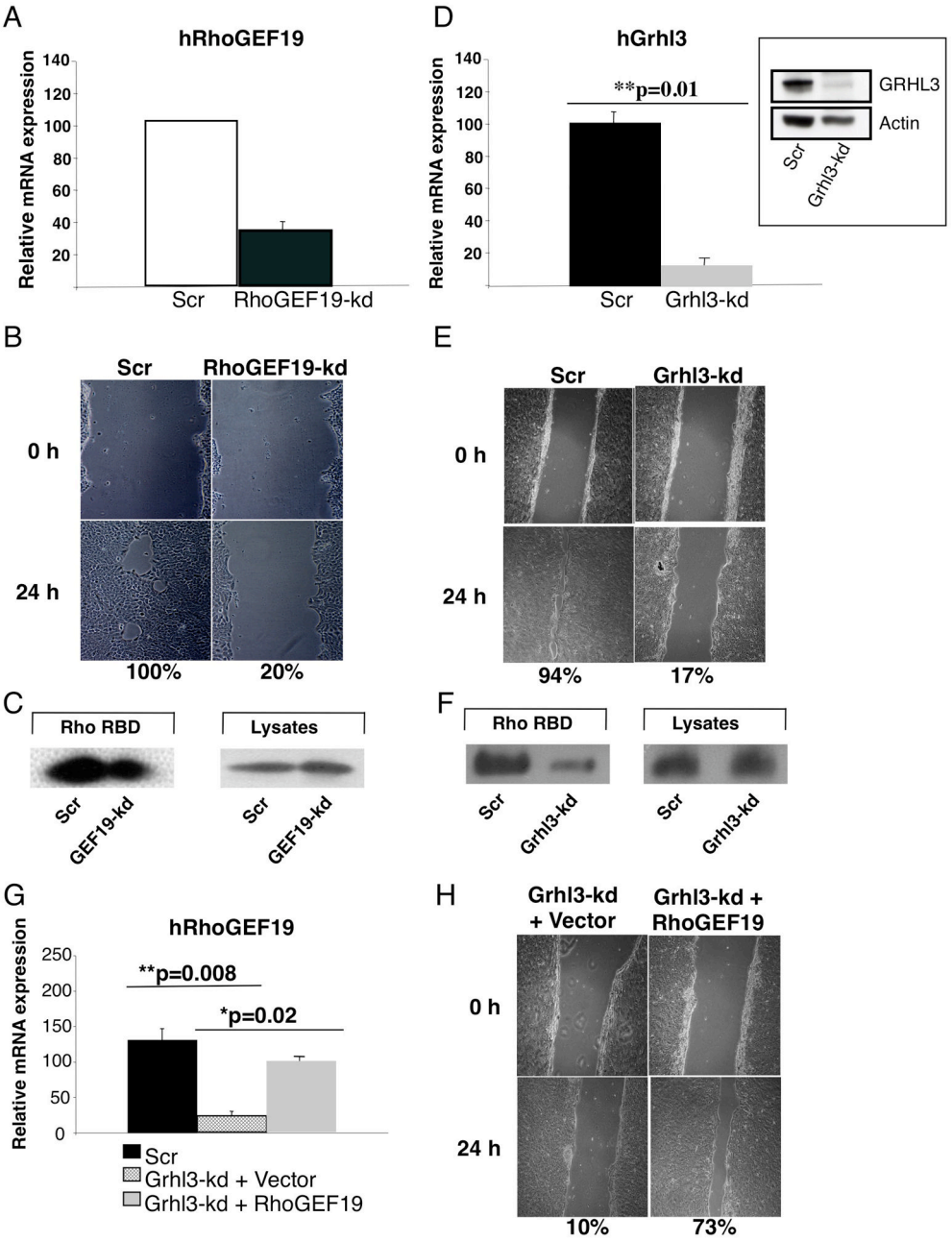

Figure 4.

Re-expression of *RhoGEF19* rescues the wound healing defect in *Grhl3*-deficient keratinocytes. (A) Q-PCR of *RhoGEF19* expression in Scr and *RhoGEF19*-kd HaCAT cells. (B) *In vitro* scratch wound assays in Scr and *RhoGEF19*-kd HaCAT cells. Percentages indicate the extent of closure compared to the original defect. (C) RhoA activation in Scr and *RhoGEF19*-kd HaCAT cells as detailed in Figure 3E. (D) Q-PCR of *Grhl3* expression in Scr and *Grhl3*-kd HaCAT cells. Inset: Western blot of GRHL3 and actin levels in Scr and *Grhl3*-kd HaCAT cells. (E) *In vitro* scratch wound assays in Scr and *Grhl3*-kd HaCAT cells. (F) RhoA activation in Scr and *Grhl3*-kd HaCAT cells. (G) Q-PCR of *RhoGEF19* expression in Scr, *Grhl3*-kd cells transduced with empty vector, and *Grhl3*-kd cells transduced with *RhoGEF19* expression vector. (H) *In vitro* scratch wound assays in *Grhl3*-

kd cells transduced with empty vector, and *Grhl3*-kd cells transduced with *RhoGEF19* expression vector. See also Figure S4.

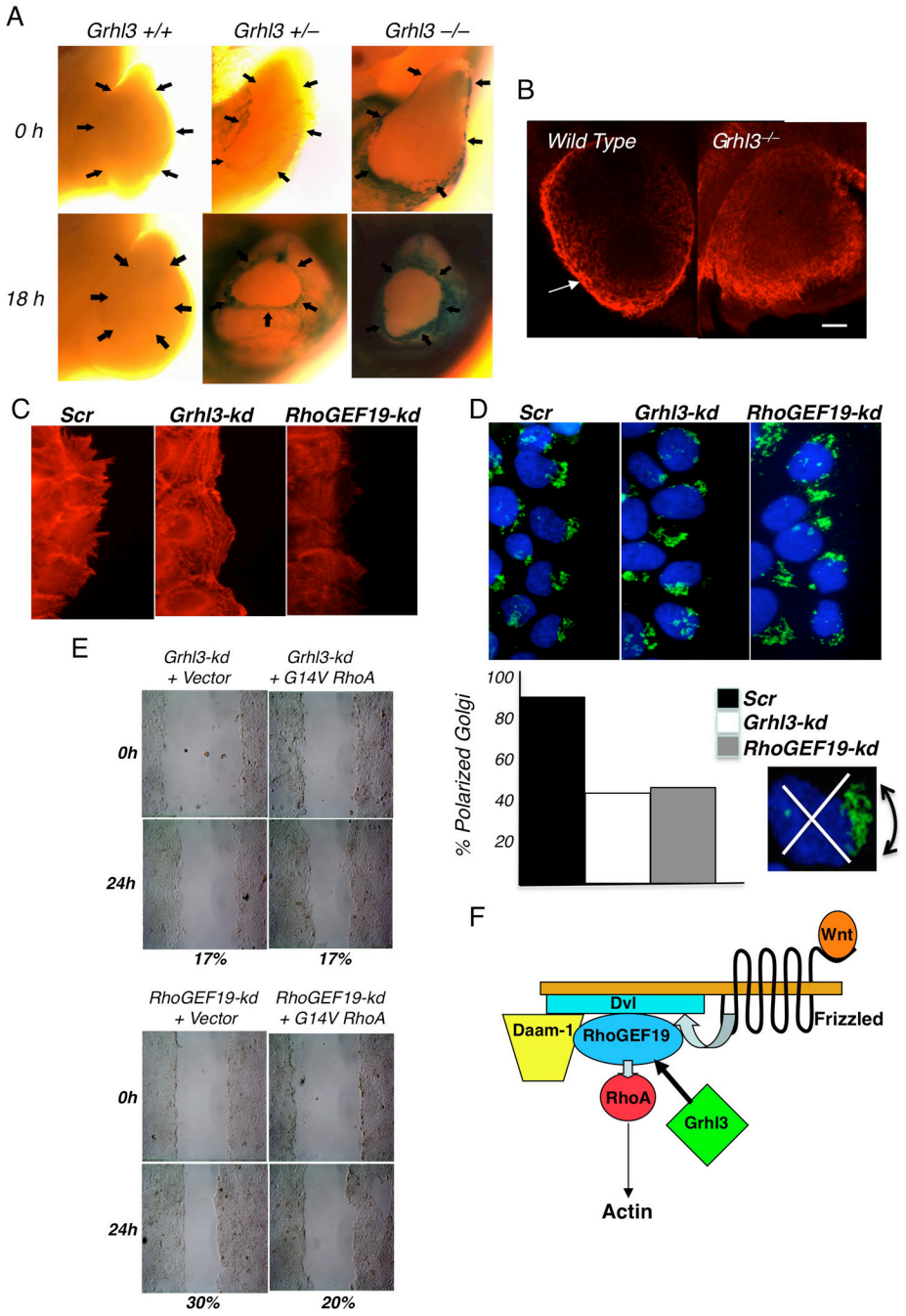

Figure 5.

Defective actin polymerization and cellular polarity in keratinocytes lacking *Grhl3* or *RhoGEF19*. (A) *LacZ* staining of hind-limb amputation wounds in *Grhl3*$^{+/+}$, *Grhl3*$^{+/-}$, and *Grhl3*$^{-/-}$E12.5 embryos at 0 and 18 hours. The arrows indicate the wound margins. (B) Whole mount phalloidin staining of F-actin cable formation in hind-limb amputation wounds in wild type and *Grhl3*$^{-/-}$E12.5 embryos at 18 hours. Scale = 100μm. (C) Phalloidin staining of scratch wound margins at 12 hours in cultured *Grhl3*-kd, *RhoGEF19*-kd, or Scr control keratinocytes. (D) *Grhl3*-kd, *RhoGEF19*-kd, or Scr keratinocytes were scratch wounded and fixed 6 hours later, prior to labeling with GM130 antibody to stain the Golgi (green) and TOPRO3 to label nuclei (blue). Shown beneath is the quantitation of cells at the

leading edge with the Golgi polarized within a 120^0 arc (inset) in front of the nucleus. (E) *Grhl3*-kd or *RhoGEF19*-kd keratinocytes were transfected with a mammalian expression vector carrying a *myc*-tagged constitutively active RhoA (G14V RhoA), or the empty vector, prior to scratch wounding and culture for 24 hours. Percentages indicate the extent of closure compared to the original defect. (F) Model of the role of *Grhl3* in PCP signaling (adapted from Tanegashima *et al.* 2008). See also Figure S5.

Table 1

Summary of wound healing data in PCP mutant strains

Genotype	No. of embryos	Open	Closed	Embryonic stage
Wild type	12	2	10	E12.5
Vangl2$^{+/-}$	9	2	7	E12.5
Vangl2$^{-/-}$	6	1	5	E12.5
Vangl2$^{+/+}$/Grhl3$^{+/-}$	7	0	7	E12.5
Vangl2$^{+/-}$/Grhl3$^{+/+}$	6	1	5	E12.5
Vangl2$^{+/-}$/Grhl3$^{+/-}$	11	9*	2	E12.5
Wild type	6	0	6	E16.5
Vangl2$^{+/-}$/Grhl3$^{+/-}$	5	0	5	E16.5
Vangl2$^{+/-}$/Grhl3$^{+/-}$	4	1	3	E16.5
Vangl2$^{+/-}$/Grhl3$^{+/-}$	7	6*	1	E16.5
Wild type	8	1	7	E12.5
Scrb1$^{+/-}$	10	2	8	E12.5
Scrb1$^{-/-}$	9	7*	2	E12.5
Scrb1$^{+/+}$/ Grhl3$^{+/-}$	10	1	9	E12.5
Scrb1$^{+/-}$/ Grhl3$^{+/+}$	9	1	8	E12.5
Scrb1$^{+/-}$/ Grhl3$^{+/-}$	7	6*	1	E12.5

* $p<0.05$